Valleriite-containing ore from Kingash deposit (Siberia, Russia): Mössbauer and X-ray photoelectron spectroscopy characterization, thermal and interfacial properties

Yuri Mikhlin [1,*], Maxim Likhatski [1], Alexander Romanchenko [1], Sergey Vorobyev [1], Yevgeny Tomashevich [1], Olga Fetisova [1], Oleg Bayukov [2], Yuriy Knyazev [2], Ivan Nemtsev [3], Sergey Karasev [1], Anton Karacharov [1] and Roman Borisov [1]

[1] Institute of Chemistry and Chemical Technology, Krasnoyarsk Science Center of the Siberian Branch of the Russian Academy of sciences, Akademgorodok, 50/24, Krasnoyarsk, 660036, Russia
[2] Kirensky Institute of Physics, Krasnoyarsk Science Center of the Siberian Branch of the Russian Academy of sciences, Akademgorodok 50/38, Krasnoyarsk, 660036, Russia
[3] Krasnoyarsk Science Center of the Siberian Branch of the Russian Academy of sciences, Akademgorodok 50, Krasnoyarsk, 660036, Russia
* Correspondence: yumikh@icct.ru; yumikh@mail.ru

Abstract: Valleriite, $(Cu,Fe)S_2 \cdot n(Mg,Al,Fe)(OH)_2$, and related layered minerals are of interest due to their unusual two-dimensional structure, formation mechanisms, physical and chemical properties, and potential involvement into mineral processing and materials science applications. Here, we have studied Kingash Cu-Ni ore samples containing 10-25% of valleriite in association with serpentines (lizardite and chrysotile) and magnetite using scanning electron microscopy and electron microprobe analysis, Mössbauer spectroscopy, X-ray photoelectron spectroscopy (XPS), thermal analysis and zeta potential measurement. The data are compared with those for Al-doped valleriite synthesized via a hydrothermal route. It was found that the Kingash valleriite contains excessive iron relative to $CuFeS_2$ stoichiometry, which mainly occurs, leaving aside magnetite, as Fe^{3+}-OH species in hydroxide layers of valleriite and minor Fe centers in serpentines. Thermal dihydroxylation of hydroxide layers of valleriites occurs near 500 ^{o}C in inert atmosphere; in air, sulfide sheets oxidize with an exothermal peak at 447 ^{o}C, and sulfur oxides don't volatilize but react with hydroxide groups of valleriite rather than serpentines. Zeta potential measurements of coarse ore particles using the flow potential technique suggested that the surface of valleriite is negatively charged in a wide pH range while the positive values at low pHs for fine particles are inflicted by serpentine. The findings demonstrate close resemblance of the natural and synthetic Al-doped valleriites, and the key role of valleriite, despite its moderate content, for the interfacial characteristics of the valleriite-bearing ores.

Keywords: valleriite; ore; two-dimensional sulfide-hydroxide composite; SEM; EDX; XPS; Mössbauer spectroscopy; thermal analysis; zeta potential

1. Introduction

Valleriite is a layered mineral composed of alternating quasi-monolayers of Cu-Fe sulfide and brucite-type hydroxide, with Al and Fe replacing a share of magnesium cations $(Mg,Al,Fe)(OH)_2$ [1-12]. The composition and characteristics of valleriites substantially depend on accompanying minerals [9-16]; moreover, some layered minerals with essentially different composition both of the sulfide and hydroxide parts have been found [17,18]. Valleriite-group minerals are rather rare but several ore deposits in Western Siberia in Russia, particularly Noril'sk "cuprous" ores [19-22] and Kingash Cu-Ni ores [23,24] contain commercial values of copper, nickel and other heavy and precious metals as valleriite and/or other minerals accompanied by valleriite. The Kingash ores located in Eastern Sayan contain pyrrhotite, pentlandite, chalcopyrite, valleriite and some other metal sulfides disseminated in ultrabasic and basic-ultrabasic intrusive rocks, and epimagmatic and hydrothermal rocks, including metamorphized varieties [25-27], with valleriite occurring in essentially serpentinized rocks. The overall resources of the deposit amount to 5.5 million tons of nickel and 2.3 million tons of copper [23], but the ores are not in commercial exploitation yet since the metal recovery by flotation is unsatisfactory [28] and no chemico-metallurgical technologies are realized as well, due to special and still poorly understood behavior of valleriite and its dense overgrowth with serpentines [28-31]. So, physical and chemical properties of valleriites as a unique two-dimensional composite material are of fundamental interest for mineral processing, Earth sciences, and materials science.

The crystalline lattice of valleriite has been established [5,7-10] to be formed by rhombohedral sulfide sublattice (space group $R\overline{3}m$) and hexagonal hydroxide sublattice (space group $P\overline{3}m1$). In the sulfide layers, Cu and Fe cations are in a distorted tetrahedral coordination with sulfide anions, and metals are in approximately octahedral environment of OH^- in the hydroxide layers. Many questions about the valleriite structure, in particular, the partition and oxidation state of Fe in both layers and the interactions between the layers, surface state and reasons of poor flotation and so forth, still need to be answered.

Recently, we explored two valleriite samples from Noril'sk ores [32,33] associated either with pyrrhotite or serpentine and chalcopyrite using X-ray absorption spectroscopy, X-ray photoelectron spectroscopy (XPS), Mössbauer spectroscopy and other techniques. Also, we managed to perform a successful hydrothermal synthesis of single-phase valleriite nanoflakes [34]. The differences observed between the valleriite samples depended on their origin in case of natural valleriites and the proportions of precursors used in the synthesis. It was established, among other things, that Mössbauer signals of paramagnetic Fe^{3+} almost disappeared and the internal hyperfine magnetic fields arose due to magnetic ordering at cryogenic temperatures; no clear signatures of ferrous iron were found in both layers [33,34], in contrast to previous studies [12,35-37].

In this contribution, the samples originated from the Kingash ore deposit were examined applying SEM/EDX, XRD, Mössbauer spectroscopy, XPS in conjunction with their thermal behavior and zeta-potential measurement. To elucidate small contributions of valleriite, the results have been compared with those for a similar synthetic phase. The aim was to reveal specific features of the mineral co-existing with high concentrations of serpentines and magnetite, in order to shed more light onto the structure and properties important for potential mineral processing and materials science applications of valleriite.

2. Materials and Methods

Kingash rock samples were obtained from the Museum of Geology of Central Siberia (Krasnoyarsk, Russia). Mineral assembles containing valleriite, which form 2-5 mm thick coatings above rock-forming minerals (Figure 1), were separated by a diamond saw. The results presented below are obtained either from the natural growth surfaces (XPS, SEM/EDX), or from the specimens ground in a jasper mortar to the particle size less than 44 μm (for XRD, Mössbauer spectroscopy, thermal analysis); a fraction with the particle size -125 +75 μm was used in zeta potential measurement. Synthetic valleriite was prepared as flakes about 100-200 nm in lateral dimensions and 10-20 nm thick using a hydrothermal reaction at 160 °C; detailed characteristics of the material can be found in ref. [34].

Figure 1. Photos of a typical rock slab (left: upper view of valleriite and accompanying minerals, right: side view showing the thickness of the upper valleriite-bearing layer.

Scanning electron microscopy (SEM), backscattered electron imaging microanalysis (SEM–BSE), and energy dispersive X-ray analysis (EDX) studies were preformed utilizing a Hitachi TM4000 Plus instrument (Hitachi High-Tech Corp., Japan) operated at acceleration voltage of 15 kV, equipped with a XFlash 630Hc EDS analyzer (Bruker, Germany). X-ray powder diffraction patterns were obtained using a PANalytical X'Pert Pro diffractometer (Eindhoven, The Netherlands) with Cu Kα radiation (30 mA, 40 kV). The diffraction analysis, including Rietveld analysis, was conducted using the HighScore suite software (PANAlytical).

^{57}Fe Mössbauer experiments were carried out with an MC-1104Em spectrometer (Cordon, Rostov-on-Don, Russia) operating in the constant acceleration mode with triangular velocity profile. A moving 57Co(Rh) source with the activity of about 50 mCi was used. The measurements were performed in a transmission mode with powdered samples (about 3 mg/cm^2 of Fe in thickness) attached to an Al sample holder at room temperature. The width of Lorentzian lines of sodium nitroprusside was 0.24 mm/s. Isomer shifts (δ)are given relative to α-iron. The spectra composed of 512 points were processed using the UnivemMS software package.

The photoelectron spectra were recorded with a SPECS spectrometer (SPECS, Berlin, Germany) equipped with a PHOIBOS 150 MCD9 hemispherical energy analyzer using monochromatic Al Kα radiation of the dual anode X-ray tube at the analyzer transmission energy of 20 eV for the survey spectra and 10 eV for high-resolution narrow region scans. A low-energy electron source FG 20 was applied to eliminate heterogeneous electrostatic charging (an electron energy of 0.05 eV and current of 10 μA); the binding energies were calibrated against the C 1s line of the adventitious carbon (285.0 eV). Atomic concentrations of elements were calculated from survey spectra. The high-resolution spectra were fitted after subtraction of the Shirley-type nonlinear background with the Gauss-Lorentz peaks utilizing the CasaXPS software package (version 2.3.16, Casa Software, Teignmouth, UK).

The thermogravimetric (TG/DTG) measurement and differential scanning calorimetric (DSC) analyses were performed in an interval from ambient temperature to 1000 ºC using a STA449 F1 Jupiter instrument (Netzsch, Germany) at a heating rate of 10 ºC/min in inert (Ar) and oxidative (N$_2$ 80% O$_2$ 20%) gas flow with a rate of 50 mL/min.

Zeta-potentials were measured employing an electrokinetic analyzer SurPASS 3 (Anton Paar, Graz, Austria) from the mineral fraction -125+75 um. The 0.01 M KCl solution was used as background electrolyte adjusted to a required pH with 0.01 M solutions of sodium hydroxide and hydrochloric acid starting both from an initial pH values of 3.0 and 10.5. The samples were equilibrated with the solution in three rinsing cycle, and then four measurement cycles were conducted at each pH value. The measurements were also carried out with ore samples ground to -20 um and synthetic valleriite colloids using the electrophoretic method with a Zetasizer Nano instrument (Malvern, Great Britain).

3. Results

3.1. XRD, SEM and EDX analysis

X-ray diffraction patterns (Figure 2) show that the major component of the rock samples are serpentine group minerals lizardite and chrysotile having similar composition Mg$_3$(Si$_2$O$_5$)(OH)$_4$ and crystalline structure [38-41], and weaker reflections of valleriite and magnetite. The diffraction

pattern of valleriite well agrees with the literature data [5-10] and that of synthetic material (pattern b) [34]. The most characteristic and clearly discernible features of valleriite are the (003) and (006) reflections [5-10,] while the other ones may overlap with those from serpentines and/or shifted owing to various composition and morphology of crystals. The Rietveld analysis of the diffractogram found the concentrations of serpentines, valleriite and magnetite phases of 81, 14, and 5 wt.%, respectively; in general, the content of valleriite ranged from 10 to 25 wt.% for various specimens examined.
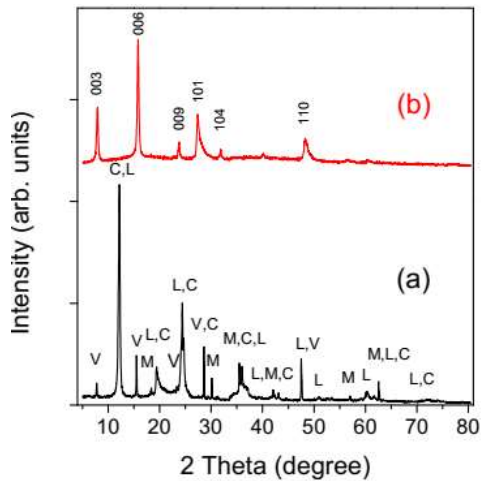

Figure 2. X-ray diffraction pattern of (a) Kingash valleriite ore in comparison with (b) synthetic valleriite (the main interplanar distances are denoted). Reflections from mineral phases are marked as V belong to valleriite (PDF 01-073-0517), M is magnetite (01-089-3854), L is lizardite-1T high (01-089-6206), C is chrysotile (00-010-0380).

Figure 3 shows a representative scanning electron microscopy image and elemental maps of the natural growth surface of a valleriite-containing rock sample; the results of microprobe analysis in selected spots are presented in Table 1. The images demonstrate a micrometer-scale intergrowth of three main minerals. The composition in spots (1) and (2) is characteristic of valleriite, though with an excess of iron. The average composition can be described by a formula $Cu_{0.87}Fe_{1.45}S_2 \cdot Mg_{1.42}Al_{0.21}Si_{0.28}(OH)_{4.48}$. Noteworthy, Si is usually all but absent in valleriites [4,11] so Si can be due to minor inclusions of gangue phases and contaminations, probably together with insignificant amounts of Al, O, Mg and Fe. The composition of the most abundant phase (spot 3) with the Mg/Si atomic ratio of 1.6 is close to the nominal formula of lizardite and chrysotile $Mg_3(Si_2O_5)(OH)_4$ [38-41]. A number of crystals (e.g., point 4) of 5-20 μm in size are composed of magnetite Fe_3O_4.

**Table 1**. Chemical composition (at. %) determined using microprobe EDX analysis.

	Fe	Cu	S	O	Mg	Al	Si	Phase
Spot 1	13.8	8.8	18.9	40.6	13.0	2.1	2.6	valleriite
Spot 2	13.2	7.4	18.4	43.1	13.4	1.9	2.6	valleriite
Spot 3	2.2	0.3	0.6	64.2	19.0	2.0	11.8	serpentine
Spot 4	28.0	3.1	8.2	48.9	9.4	0.5	1.9	magnetite
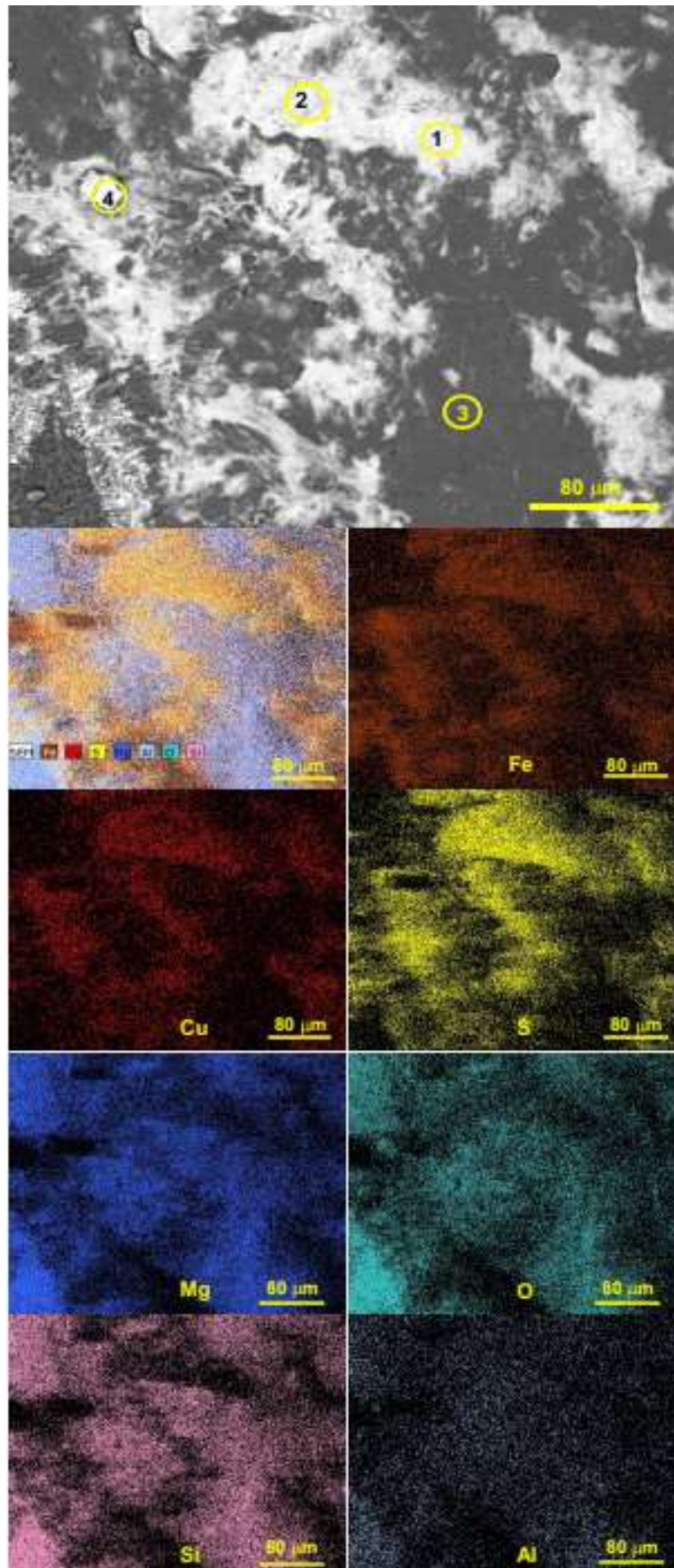
Figure 3. Scanning microscopy image and elemental maps of natural growth surface of a typical valleriite-containing rock sample from Kingash deposit. Numbers in SEM image designate spots whose composition is presented in Table 1.

3.2. Mössbauer spectroscopy

[57]Fe Mössbauer spectroscopy is a powerful element-specific method that allows discriminating the chemical states of Fe atoms and magnetic ordering in various phases [12,33-37,42-44]. Typical Mössbauer spectrum of the valleriite-bearing samples (Figure 4; Table 2 represents fitting parameters) consists of two intense Zeeman sextets with the ratio close to 1:2 and hyperfine parameters well agreed with the ones of magnetite Fe_3O_4 [42-44]. The first sextet s1 originates from Fe^{3+} cations located in the tetrahedral positions and the second one (s2) is due to Fe^{2+} and Fe^{3+} cations in octahedral coordination with O^{2-} anions (denoted as $Fe^{2.5+}(6O)$ in Table 2) that are not resolved in the spectra because of fast electron hopping. The smeared third sextet s3 is most likely due to diamagnetic dilution in magnetite, possibly with Al and Mg.
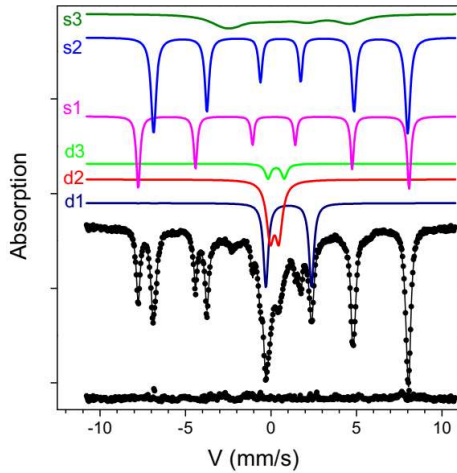
Figure 4. [57]Fe Mössbauer spectrum (points) of a Kingash rock sample measured at room temperature. The lines are the results of fitting; the difference between experimental spectrum and and fitted one also shown was typically within 3 rel.% of the spectrum area. The fit parameters are given in Table 2.

Table 2. The [57]Fe Mössbauer parameters of valleriite-containing Kingash sample and synthetic valleriite measured at 300 K. δ is the isomer shift relative to α-Fe (mm/s), Δ is the quadrupole splitting (mm/s) with the doubled quadrupole shift ($\Delta = 2\varepsilon$) given for magnetically split components, W_{34-16} is the width of absorption lines (mm/s), H_{eff} is the internal magnetic field (kOe), A is the relative area of a spectrum component.

	$\delta\pm0.01$	$H_{eff}\pm5$	$\Delta\pm0.02$	$W_{34-16}\pm0.02$	$A\pm5$ (%)	Cation(position)	Phase
				Kingash ore sample			
s1	0.27	493	-0.04	0.22-0.26	19	$Fe^{3+}(4O)$	magnetite
s2	0.67	463	0.02	0.26-0.36	33	$Fe^{2.5+}(6O)$	magnetite
s3	0.57	230	3.64	1.83-2.02	17	$Fe^{2.5+}(6O)$	magnetite
d1	1.15	-	2.67	0.34	14	$Fe^{2+}(6O,OH)$	serpentine
d2	0.32	-	0.53	0.52	14	$Fe^{3+}(4S)$	valleriite
d3	0.41	-	0.96	0.39	3	$Fe^{3+}(6O,OH)$	valleriite, serpentine
				synthetic Al-doped valleriite [33]			
d1	0.36	-	0.57	0.40	78	$Fe^{3+}(4S)$	valleriite
d2	0.42	-	1.02	0.26	22	$Fe^{3+}(6O)$	valleriite

The hyperfine parameters of the first of three doublets (d_1) with isomer shift δ of 1.15 mm/s and quadrupole splitting Δ of 2.67 mm/s are typical for ferrous iron in octahedral coordination with oxygen; in particular, similar values have been found for Fe^{2+} cations in serpentines [39-42]. Chistyakova et al. [35] have detected such small feature for synthetic valleriite-containing products and assigned it to di- and trivalent iron in the hydroxide layers but we didn't observe this doublet in pure valleriites [34]. The second doublet with δ of 0.32 mm/s and $\Delta = 0.5$ mm/s is attributed to

Fe^{3+} cations in tetrahedral coordination with sulfide anions in valleriite [12,33-37] as it is close to the species in synthetic valleriite (Table 2) and clearly differs from Fe^{3+} tetrahedrally bounded to oxygen in serpentines, for which δ of about 0.16 mm/s and Δ of 0.25-0.42 mm/s have been reported [39-42]. A smaller paramagnetic doublet with the isomer shift $\delta \sim 0.4$ mm/s and quadrupole splitting of 0.96 mm/s observed both in synthetic and natural valleriites [12,33-37] can be assigned to octahedral Fe^{3+}-OH sites in the hydroxide layers and partially in serpentines [39-42]. The excess of Fe found in spots 1 and 2 (Figure 2) suggests that up to 30-40% of the iron in valleriite occurs in the hydroxide layers.

3.3. X-ray photoelectron spectroscopy

XPS determines the composition of near-surface mineral region of few nanometers in depth, averaged over the sample surface because of the lack of lateral resolution; the high-resolution spectra provide information on oxidation state and chemical bonding of specific elements. The concentrations of elements at the ore surface presented in histogram (Figure 5) are in a reasonable agreement with the EDX data, with the contents of Cu and S being more than twice lower in comparison with synthetic valleriite, as these elements are absent in other minerals. In both samples, the photoelectron Cu $2p_{3/2}$ peak with the binding energy (BE) of ~932.5 eV and no shake-up satellites at 944-948 eV, as well as the position of Auger L_3MM line at 917 eV are indicative of sulfur-bonded copper +1 species in the sulfide layers of valleriite, with some broadening at the BEs of 933-936 eV being due to a minor contribution of oxidized copper species or/and "shake-off" satellites [32,33,45-47]. The position of the major S $2p_{3/2}$ peak at 161.7 eV is characteristic of monosulfide in valleriites [32-34]. The spectra are better fitted using contributions of disulfide (162.5 eV) and polysulfide (163.4 eV) and a satellite at ~164.5 eV similar to bulk Cu-Fe sulfides [45-47]. The small intensities of the di- and polysulfide components with the sum intensity of 10% total sulfur together with negligible concentrations of sulfate and other oxysulfur species (BE above 167 eV) imply insignificant oxidation of the sulfide sheets enclosed by hydroxide layers in the natural and synthetic minerals.
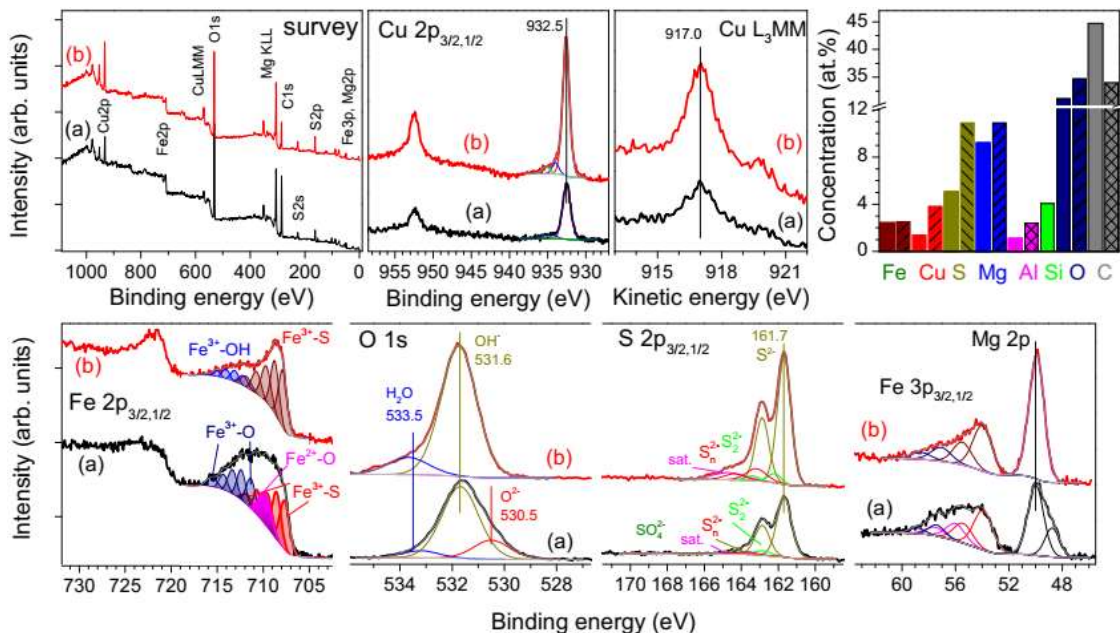
Figure 5. X-ray photoelectron spectra, and atomic concentrations (histogram) derived from the survey spectrum for (a) Kingash valleriite-containing sample and (b) synthetic valleriite (patterned columns in the concentration histogram).

The Fe 2p spectra include contributions from several phases and species, each of them exhibiting multiplet sets of lines [48,49]. While the spectra of pure valleriite can be well fitted with two five-line sets for Fe^{3+}-S (first peak at 707.8 eV) and Fe^{3+}-OH (~711 eV) species, at least one more maximum centered at the BE of 709.8 eV with the intensity of 15-20 rel.% attributable to

high-spin O-bonded Fe^{2+} should be added for the ore samples. Correspondingly, the Fe 3p spectra can be deconvoluted using two or three doublets centered at ~54 eV (Fe-S species), 55.4 eV (Fe^{2+}-O) and ~57 eV (Fe^{3+}-O). Both Fe 2p and 3p spectra confirm, therefore, that Fe^{2+} species occurs in the Kingash rock sample but absent in synthetic valleriite. Some difference in the component intensities is likely due to surface oxidation as the probing depth for Fe 3p spectra is larger by a factor of ~1.4 than that for the Fe 2p spectral region. The signals of $Fe^{2+/3+}$ cations from magnetite appear to be small because of a low visible surface area of the Fe_3O_4 crystals (Figure 3), and the peaks of ferrous iron are mostly due to serpentines. The Mg 2p spectra show two maxima at the BEs of ~50 eV and 48.8 eV, probably from valleriite and serpentines, respectively. The main O 1s peak at 531.7 eV is due to OH groups in serpentines and valleriite and the one (about 20 rel.%) at 530.5 eV arises from O^{2-} anions in magnetite, serpentines and valleriite; a maximum at 533.2 eV originates from surface water and oxygen in carbonaceous contaminations. Consequently, the XPS shows the comparable surface areas of serpentines and valleriite and insignificant magnetite in the Kingash ore specimen. The spectra also prove that the chemical states of elements in synthetic and natural valleriites are very similar.

3.4. Thermal behavior

The thermal reactions of valleriites are of interest for understanding the mechanisms of mineral formation, stability, ore processing and for material applications. Heating the rock sample in inert environment (Figure 6, a) results in minor endothermal effects and loss of about 1.3 % of total weight in the temperature range from 460 °C to 580 °C which may be due transformation of serpentines and valleriite releasing water from the hydroxide layers. Valleriite has been reported to be generally stable up to the temperature of 600-650 °C [13,50] while lizardite and chrysotile are known to gradually dehydroxilate through a wide temperature interval [51-53], masking the reactions of valleriite. Synthetic valleriite (Figure 6, c) exhibits desorption of water starting from ~50 °C, the endothermal reaction occurring at ~500 °C and a smaller second step at about 580 °C. Similar processes in brucite correspond to the formation of defect MgO keeping the structure and residual OH groups and finally of the cubic bulk MgO [54], though at lower temperatures. Hence, minor features discerned for the natural samples near 500 °C (Figure 6, a) can be attributed to the reactions of valleriite, i.e., transformation of metal hydroxide layers to metal oxides releasing water. Bulk decomposition of serpentines in the Kingash sample with the loss of about 11 wt.% peaked at 723 °C and a second stage started at 900 °C.

The ore sample heated in the oxidative atmosphere shows (Figure 6, b) an exothermic peak at 447 °C associated with an increase in the sample weight by ~4% and a smaller stage at ~510 °C. The pure valleriite reveals the major maximum at 496 °C with two minor reactions at 346.6 and about 620 °C. Li and Cui [9] have observed similar effects starting from 480 °C and described those as "a structural change and the formation of a new phase". It is clear that these effects are related to oxidation of sulfide yielding SO_2/SO_3 and their reactions with (hydr)oxide layers (or products of their dehydroxilation) in valleriite producing metal sulfates; the exact mechanisms of the reactions still need to be understood. It is worth underlining that no or very minor sulfur species are released into the environment from the sulfide sheets confined by hydroxide layers of the composite mineral, and the role of surrounding serpentines is insignificant. The endothermic transformations of serpentines losing OH/H_2O are somewhat shifted in air as compared with inert atmosphere.
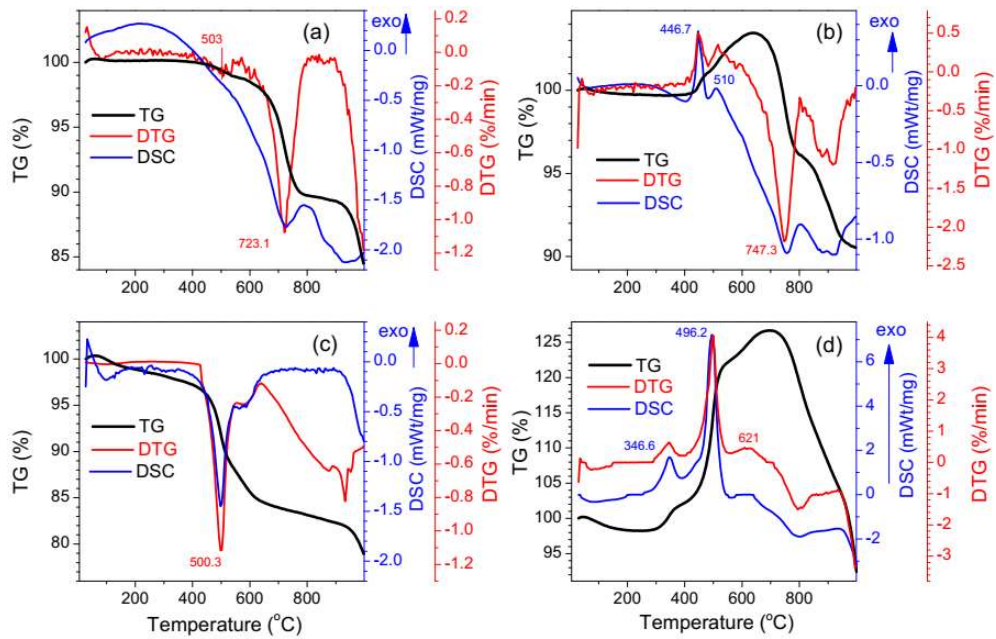
Figure 6. Thermogravimetric (TG), differential thermogravimetric (DTG), and differential scanning calorimetry (DSC) curves for heating (a),(b) valleriite-containing Kingash sample and (c),(d) synthetic valleriite in (a),(c) inert Ar and (b),(d) air flow.

3.5. Zeta potential

Zeta potential is an important indicator of the state of solid/aqueous interfaces. Hydrophilic magnesium serpentines and brucite [29-31,55,56] are known to have positive zeta potentials in pH interval of 7-11 important for froth flotation, adhering to negatively charged sulfide mineral surfaces and suppressing their flotation recovery [28-31]. One could expect that valleriites exposing brucite-like outermost layers at the interface also has an isoelectric point at the pH about 11 [55], and, moreover, Al^{3+} cations substituting Mg^{2+} induce a positive charge of hydroxide layers whereas sulfide sheets are charged negatively [8-10]. The experiments performed with synthetic valleriites, however, found an opposite trend [34], with the submicrometer flakes having negative zeta potentials almost independent on pH (Figure 7, curve a).
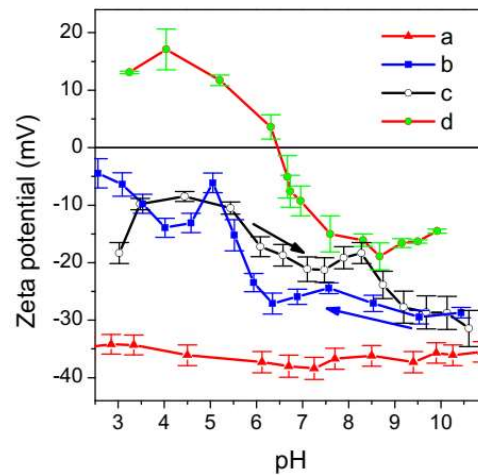
Figure 7. Zeta potentials of (a) synthetic valleriite nanoflakes and Kingash ore samples measured using (b,c) the flow potential method from the fraction -125 + 75 μm with (b) increasing and (c) decreasing pH and (d) electrophoretic mobility for the fraction -20 μm.

In the current research, zeta potentials vs pH plots for the Kingash ore samples were determined by measuring the flow potentials (plots b, c) of rather coarse, from 75 to 125 μm, particles, in comparison with the conventional electrophoretic measurements (plots a,d) involving

much finer particles, in order to elucidate the contributions of valleriite and serpentine entities. Zeta potentials of the coarse ore particles are generally negative although the magnitude between -10 mV and -25 mV is lower than that of the synthetic phase. The potential values depend also on the direction of pH changing; the negative magnitude is larger in the case of decreasing pH but it reduces at pH < 5. The plot (d) acquired using electrophoretic method from fine ore particles show an isoelectric point near pH 6.5. These findings imply that valleriite in the Kingash rocks has negative zeta potentials similar to synthetic phase, and the positive charge is imposed by fine serpentine particles, mainly at lower pHs.

4. Discussion and Conclusions

Valleriite in the Kingash rock samples is associated with serpentines and magnetite but not sulfide minerals, in contrast, for example, to valleriite ores from Noril'sk deposits [32,33]. It contains excessive, relative to the $CuFeS_2$ stoichiometry, iron that occurs mainly as Fe^{3+} cations in brucite-like hydroxide layers substituting Mg^{2+}. The Kingash mineral appears close to Noril'sk valleriite associated with pyrrhotite and magnetite in absence of serpentines rather than the one associated with chalcopyrite and lizardite that is a product of incomplete reaction between Cu-bearing sulfides and serpentines and contains lower Fe in hydroxide layers. The Fe^{3+}-O as well as Al^{3+}-O species unexpectedly induced a more negative rather than positive, electric charge of the hydroxide sheets and so positive charge of the sulfide part, and negative zeta potential, similarly to synthetic material [34]. Mössbauer spectra show, apart from Zeeman sextets of magnetite, three doublets of paramagnetic Fe. The comparison with EDX and XPS data, previous studies [12,33] and synthetic valleriite [34] allows to conclude that the doublet with $\delta \approx 0.30$ mm/s and quadrupole splitting Δ of ~0.56 mm/s is due to Fe^{3+} sites in the sulfide sheets of valleriite. The feature with $\delta = 1.14$ mm/s and $\Delta = 2.64$ mm/s appears to originate from ferrous iron in serpentines. The third, lower, doublet is attributable to oxygen-bonded ferric iron in valleriite and partially in serpentines. The photoelectron spectra of Fe revealed contributions of S- and O-bonded ferric iron, originating mostly from valleriite, and Fe^{2+} in serpentines. The spectra of sulfur and copper are very similar for natural and synthetic valleriites.

Thermal analysis experiments showed that sulfide part of valleriite oxidizes in air at 447 ºC with exothermic effect and an increase in the sample weight, so sulfur confined between the hydroxide layers doesn't volatilize as SO_2 or S. In inert atmosphere, the samples decay yielding water in endothermic reaction(s) at about 500 ºC both for natural and synthetic valleriites. The temperatures of the non-oxidative and oxidative decomposition are close, suggesting that sulfur oxides appear to react with metal hydroxide layers and their decomposition products rather than with serpentines. The decomposition temperatures are lower than those for serpentines, and this may be employed for chemical separation and extraction of metal values.

Zeta potentials measured using the flow potential method at rather big particles imply that valleriite surfaces are negatively charged; positive zeta potentials found utilizing electrophoretic techniques and finely ground minerals are due to serpentine particles. The characteristics of the ore surfaces are substantially affected by valleriite, despite its content is lower than that of serpentines, possibly due to its easier exfoliation. The experiments suggest that higher pH in the flotation or pretreatment with alkaline solutions may promote the recovery of valleriite from serpentine-rich ores. The results should be taken into consideration for developing technologies of mineral beneficiation and chemical processing of the Kingash ores or similar resources.

Author Contributions: conceptualization, Y.M.; methodology, Y.M., O.B., M.L., A.R.; investigation, Y.M., A.R., S.V., M.L., Y.T., O.B., Y.K., O.F.; I.N., S.K., R.B., A.K.; resources, Y.M., A.R., S.K.; data curation, M.L., O.B., O.F., Y.T.; writing—original draft preparation, A.R., Y.M.; writing—review and editing, Y.M., O.B.; visualization, Y.M., A.R., O.B., I.N.; supervision, Y.M.; project administration, Y.M.; funding acquisition, Y.M.

References

1. Chamberlain, J.A., Delabio, R. N. Mackinawite and valleriite in the Muskox intrusion. *Am. Mineral*. **1965**, *50*, 682-695.
2. Cabri, L.J. A new copper-iron sulfide. *Econ. Geol.* **1967**, *62*, 910-925. https://doi.org/10.2113/gsecongeo.62.7.910.
3. Genkin, A. D.; Val'sov, L. N. O Valleriite i machinovite i usloviyakh ikh nakhozhdeniya v rudakh (On valleriite and makhinovite and conditions of their presence in ores). *Geol. Rud. Mestorozhd*. 1967, 9 (2), 94-106 (in Russian).
4. Springer, G. Electronprobe analyses of mackinawite and valleriite. *Neues Jahrb. Mineral. Monatsh.* **1968**, *8*, 252-258. http://pascal-francis.inist.fr/vibad/index.php?action=getRecordDetail&idt=GEODEBRGM6801021781.
5. Evans, H.T. Jr., Allman, R. The crystal structure and crystal chemistry of valleriite. *Z. fur Kristallogr*. **1968**, *127*, 73-93. https://doi.org/10.1524/zkri.1968.127.1-4.73.
6. Petruk, W., Harris, D.C., Murray, E.J. An occurrence of valleriite from New Imperial Mine, Yukon. *Can. Mineral*. **1971**, *10*, 885-888.
7. Organova, N.I. Crystallochemistry of modulated and incommensurate structures in minerals. *Int. Geol. Rev.* **1986**, *28*, 802-814. https://doi.org/10.1080/00206818609466322.
8. Hughes, A.E., Kakos, G.A., Turney, T.W., Williams, T.B. Synthesis and structure of valleriite, a layered metal hydroxide/sulfide composite. *J. Solid State Chem.* **1993**, *104*, 422-436. https://doi.org/10.1006/jssc.1993.1178
9. Li, R., Cui, L. Investigations on valleriite from Western China: crystal chemistry and separation properties. *Int. J. Miner. Process*. **1994**, *41*, 271-283. https://doi.org/10.1016/0301-7516(94)90033-7.
10. Qin, S.; Cao, Z.; Chen, Y. Preliminary study on crystal chemistry of valleriite. *Chin. Sci. Bull.* **1996**, *41*, 1982-1985.
11. Mücke, A. Review on mackinawite and valleriite: formulae, localities, associations and intergrowths of the minerals, mode of formation and optical features in reflected light. *J. Earth Sci. Clim. Change* **2017**, *8*, 1000419. https://doi.org/10.4172/2157-7617.1000419.
12. Waanders, F.B., Pollak, H. Mössbauer spectroscopy to characterize iron sulphides. *South Afr. J. Sci.* **1999**, *95*, 387-390.
13. Harris, D.C., Vaughan, D.J. Two fibrous iron sulfides and valleriite from Cyprus with new data on valleriite. *Am. Mineral*. **1972**, *57*, 1037–1052.
14. Harris, D.C., Cabri, L.J., Stewart, J.M. A "Valleriite-type" mineral from Noril'sk, Western Siberia. *Am. Mineral*. **1970**, *55*, 2110-2114.
15. Nickel, E.H., Hudson, D.R. The replacement of chrome spinel by chromian valleriite in sulphide-bearing ultramafic rocks in Western Australia. *Contrib. Mineral. Petrol*. **1976**, *55*, 265-277. https://doi.org/10.1007/BF00371337.
16. Pekov, I.V., Sereda, E.V., Yapaskurt, V.O., Polekhovsky, Y.S., Britvin, S.N., Chukanov, N.V. Ferrovalleriite, $2(Fe,Cu)S \cdot 1.5Fe(OH)_2$: validation as a mineral species and new data. *Geol. Ore Deposits* **2013**, *55*, 637-647. https://doi.org/10.1134/S1075701513080102.
17. Pekov, I.V., Yapaskurt, V.O., Polekhovsky, Y.S., Vigasina, M.F., Siidra, O.I. Ekplexite $(Nb,Mo)S_2 \cdot (Mg_{1-x}Al_x)(OH)_{2+x}$, Kaskasite $(Mo,Nb)S_2 \cdot (Mg_{1-x}Al_x)(OH)_{2+x}$ and Manganokaskasite $(Mo,Nb)S_2 \cdot (Mn_{1-x}Al_x)(OH)_{2+x}$, Three New Valleriite-Group Mineral Species from the Khibiny Alkaline Complex, Kola Peninsula, Russia. *Mineral. Mag.* **2014**, *78*, 663–679. https://doi.org/10.1180/minmag.2014.078.3.14.
18. Pekov, I.V., Sereda, E.V., Polekhovsky, Y.S., Britvin, S.N., Chukanov, N.V., Yapaskurt, V.O., Bryzgalov, I.A. Ferrotochilinite, $6FeS \cdot 5Fe(OH)_2$, a new mineral from the Oktyabr'sky Deposit,

Noril'sk district, Siberia, Russia. *Geol. Ore Deposits* **2013**, *55*, 567-574. https://doi.org/10.1134/S1075701513070106.

19. Genkin, A. D.; Distler, V. V.; Gladyshev, G. D. *Sul'fidnye Medno-Nikelevye Rudy Noril'skikh Mestorozhdenii (Sulphidic Copper-Nickel Ores of Noril'sk Deposits)*. Nauka, Moscow, 1981. 234 p. (in Russian).

20. Dodin, D.A. *Metallogeniya Taimyro-Noril'skogo Regiona (Metallogeny of Taimyr-Noril'sk Region)*. St.-Petersburg, Nauka, 2002. 374 p. (in Russian).

21. Laptev, Yu. V.; Shevchenko, V. S.; Urakaev, F. Kh. Sulphidation of valleriite in SO_2 solutions. *Hydrometallurgy* **2009**, *98*, 201–205. https://doi.org/10.1016/j.hydromet.2009.04.018.

22. Krivolutskaya, N.A. Siberian Traps and Pt-Cu-Ni Deposits in the Noril'sk Area, Springer Cham Heidelberg New York Dordrecht London. 2016. 364 p. https://doi.org/10.1007/978-3-319-17205-7.

23. Lygin, A.V. Peculiar features of ore composition of the upper Kingash PGE-Co–Cu–Ni deposit (Krasnoyarsk territory). *Moscow Univ. Geol. Bull.* **2010**, *65*, 130–133. https://doi.org/10.3103/S0145875210020092.

24. Mikhlin, Y., Romanchenko, A., Vorobyev, S., Karasev, S., Volochaev, M., Kamenskiy, E., Burdakova, E. Ultrafine particles in ground sulfide ores: A comparison of four Cu-Ni ores from Siberia, Russia. *Ore Geol. Rev.* **2017**, *81*, 1–9. http://dx.doi.org/10.1016/j.oregeorev.2016.10.024.

25. Glazunov, O.M., Radomskaya, T.A. Geochemical model of genesis of the Kingash platinoid–copper–nickel deposit. *Dokl. Earth Sci.* **2010**, *430*, 71–75. https://doi.org/10.1134/S1028334X10010162.

26. Yurichev, A.N., Chernyshov, A.I. New ore minerals from the Kingash ultramafic massif, Northwestern Eastern Sayan. *Geology of Ore Deposits*, **2017**, *59*, 626–631. https://doi.org/10.1134/S107570151707011X.

27. Algebraistova, N.K., Perfileva, N.S., Markova, S.A., Razvayznaya, A.V., Groo, E.A., Kondratieva, A.A., Macshanin, A.V., The development combinative ore-dressing scheme of Kingash ore. *J. Siberian Fed. Univ. Eng. Technol.* **2012**, 7, 777-782. http://krsk.elib.sfu-kras.ru/bitstream/2311/9534/1/10_Algebraistova.pdf (In Russian).

28. Edwards, C.R., Kipkie, W.B., Agar, G.E. The effect of slime coatings of the serpentine minerals, chrysotile and lizardite, on pentlandite flotation. *Int. J. Min. Process.* **1980**, 7, 33-42. https://doi.org/10.1016/0301-7516(80)90035-6.

29. Bremmell, K.E., Fornasiero, D., Ralston, J. Pentlandite–lizardite interactions and implications for their separation by flotation. *Colloids Surf. A* **2005**, *252*, 207–212. https://doi.org/10.1016/j.colsurfa.2004.10.100.

30. Kirjavainen, V., Heiskanen, K. Some factors that affect beneficiation of sulphide nickel–copper ores. *Miner. Eng.* **2007**, *20*, 629–633. https://doi.org/10.1016/j.mineng.2007.01.001.

31. Mikhlin, Y.L., Romanchenko, A.S., Tomashevich, E.V., Volochaev, M.N., Laptev, Yu.V. XPS and XANES study of layered mineral valleriite. *J. Struct. Chem.* **2017**, *58*, 1137–1143. https://doi.org/10.1134/S0022476617060105.

32. Mikhlin, Y.L., Likhatski, M.N., Bayukov, O.A., Knyazev, Y.V., Velikanov, D.A., Tomashevich, Y.V., Romanchenko, A.S., Vorobyev, S.A., Volochaev, M.V., Zharkov, S.M., Meira, D.M. Valleriite, a natural two-dimensional composite: X ray absorption, photoelectron and Mössbauer spectroscopy and magnetic characterization. *ACS Omega* **2021**, *6*, 7533–7543. http://dx.doi.org/10.1021/acsomega.0c06052.

33. Mikhlin, Y.L., Borisov, R.V., Vorobyev, S.A., Tomashevich, Y.V., Romanchenko, A.S., Likhatski, M.N., Karacharov, A.A., Bayukov, O.A., Knyazev, Y.V., Velikanov, D.A., Zharkov, S.M., Krylov, A.S., Krylova, S.N., Nemtsev, I.V. Synthesis and characterization of nanoscale composite particles formed by 2D layers of Cu-Fe sulfide and Mg-based hydroxide. *ChemRxiv.org.* **2022**. http://dx.doi.org/10.33774/chemrxiv-2021-9h902-v2.

34. Chistyakova, N.I., Gubaidulina, T.V., Rusakov, V.S. Mossbauer investigations of natural and synthetic tochilinite and valleriite. *Czech. J. Phys.* **2006**, *56*, E123–E131. https://doi.org/10.1007/s10582-006-0478-7.

35. Gubaidulina, T.V., Chistyakova, N.I., Rusakov, V.S. Mössbauer study of layered iron hydroxysulfides: tochilinite and valleriite. *Bull. Russ. Acad. Sci. Phys.* **2007**, *71*, 1269–1272. https://doi.org/10.3103/S106287380709016X.

36. Chistyakova, N.I., Rusakov, V.S., Gubaidulina, T.V., Gapochka, A.M., Bychkov, A.Yu. Mössbauer investigations of synthetic valleriite. *Hyperfine Interact.* **2012**, *208*, 99–104. https://doi.org/10.1007/s10751-011-0474-6.

37. Wicks, F.J., Whittaker, E.J.W. A reappraisal of the structures of the serpentine minerals. *Can. Mineral.* **1975**, *13*, 227-243.

38. O'Hanley, D.S., Dyar, M.D. The composition of lizardite 1T and, the formation of magnetite in serpentinites. *Am. Mineral.* **1993**, *78*, 391-404.

39. O'Hanley, D.S., Dyar, M.D. The composition of chrysotile and its relationship with lizardite. *Can. Mineral.* **1998**, *36*, 727-798.

40. Evans, B.W. The serpentinite multisystem revisited: chrysotile is metastable. *Int. Geol. Rev.* **2004**, *46*, 479–506. https://doi.org/10.2747/0020-6814.46.6.479.

41. Stevens, J.G., Khasanov, A.M., Miller, J.W., Pollak, H., Li, Z. (Eds). *Mössbauer Mineral Handbook.* Mössbauer Effect Data Center, Asheville, NC, **2005**, 624 p.

42. Belov, K.P. Electronic processes in magnetite (or, "Enigmas of magnetite"). *Phys.–Usp.* **1993**, *36*, 380-391. https://doi.org/10.1070/PU1993v036n05ABEH002160.

43. Dézsi, I., Fetzer, Cs., Gombkötő, Á., Szűcs, I., Gubicza, J., Ungár, T. Phase transition in nanomagnetite. *J. Appl. Phys.* **2008**, *103*, 104312. https://doi.org/10.1063/1.2937252.

44. Goh, S.; Buckley, A.; Lamb, R.; Rosenberg, R.; Moran, D. The oxidation states of copper and iron in mineral sulfides, and the oxides formed on initial exposure of chalcopyrite and bornite to air. *Geochim. Cosmochim. Acta* **2006**, *70*, 2210–2228. https://doi.org/10.1016/j.gca.2006.02.007.

45. Mikhlin, Y., Nasluzov, V., Romanchenko, A., Tomashevich, Y., Shor, A., Felix, R. Layered structure of the near-surface region of oxidized chalcopyrite ($CuFeS_2$): hard X-ray photoelectron spectroscopy, X-ray absorption spectroscopy and DFT+U studies. *Phys. Chem. Chem. Phys.* **2017**, *19*, 2749–2759. https://doi.org/10.1039/C6CP07598C.

46. Nasluzov, V., Shor, A., Romanchenko, A., Tomashevich, Y., Mikhlin, Y. DFT + U and low-temperature XPS studies of Fe-depleted chalcopyrite ($CuFeS_2$) surfaces: A focus on polysulfide species. *J. Phys. Chem. C* **2019**, *123*, 21031–21041. https://doi.org/10.1021/acs.jpcc.9b06127.

47. Grosvenor, A. P.; Kobe, B. A.; Biesinger, M. C.; McIntyre, N. S. Investigation of multiplet splitting of Fe 2p XPS spectra and bonding in iron compounds. *Surf. Interface Anal.* **2004**, *36*, 1564-1574.https://doi.org/10.1002/sia.1984.

48. Mikhlin, Y., Romanchenko, A., Tomashevich, Y. Surface and interface analysis of iron sulfides in aqueous media using X-ray photoelectron spectroscopy of fast-frozen dispersions. *Appl. Surf. Sci.* **2021**, *549*, 149261. https://doi.org/10.1016/j.apsusc.2021.149261.

49. Iiishi, K., Tomisaka, T., Kato, T., Takeno, S. Syntheses of Valleriite. *Am. Mineral.* **1970**, *55*, 2107-2110.

50. Caruso, L.J., Chernosky, J.V. The stability of lizardite. *Can. Mineral.* **1979**, *17*, 757-769.

51. Trittschack, R., Grobéty, B. The dehydroxylation of chrysotile: A combined in situ micro-Raman and micro-FTIR study. *Am. Mineral.* **2013**, *98*, 1133-1145. https://doi.org/10.2138/am.2013.4352.

52. Trittschack, R., Grobéty, B., Koch-Müller, M. In situ high-temperature Raman and FTIR spectroscopy of the phase transformation of lizardite, Am. Mineral. **2012**, *97*, 1965-1976. http://dx.doi.org/10.2138/am.2012.4162.

53. Nahdi, K., Françoise Rouquerol, F., Ayadi, M.T. $Mg(OH)_2$ dehydroxylation: A kinetic study by controlled rate thermal analysis (CRTA). *Solid State Sci.* **2009**, *11*, 1028–1034. https://doi.org/10.1016/j.solidstatesciences.2009.02.013.

54. Kosmulski, M. Isoelectric points and points of zero charge of metal (hydr)oxides: 50 Years after Parks' review. *Adv. Colloid Interf. Sci.* **2016**, *238*, 1–61. https://doi.org/10.1016/j.cis.2016.10.005.

55. Zhang, L., Mishra, D., Zhang, K., Perdicakis, B., Pernitsky, D., Lu, Q. Electrokinetic study of calcium carbonate and magnesium hydroxide particles in lime softening. *Water Research*, **2020**, *186*, 116415. https://doi.org/10.1016/j.watres.2020.116415.